Title

Microscopy ambient ionization top-down mass spectrometry reveals developmental patterning

Journal

Proceedings of the National Academy of Sciences of the United States of America, 110(37)

ISSN

0027-8424

Authors

Hsu, Cheng-Chih
White, Nicholas M
Hayashi, Marito
et al.

Publication Date

2013-09-10

DOI

10.1073/pnas.1310618110

Peer reviewed

Microscopy ambient ionization top-down mass spectrometry reveals developmental patterning

Cheng-Chih Hsu[a], Nicholas M. White[b,c], Marito Hayashi[b,c], Eugene C. Lin[a], Tiffany Poon[b,c], Indroneal Banerjee[d], Ju Chen[d], Samuel L. Pfaff[b,c], Eduardo R. Macagno[e], and Pieter C. Dorrestein[a,f,1]

[a]Department of Chemistry and Biochemistry, [d]Department of Medicine, and [e]Division of Biological Sciences, University of California, San Diego, La Jolla, CA 92093; [b]Howard Hughes Medical Institute and [c]Gene Expression Laboratory, The Salk Institute for Biological Studies, La Jolla, CA 92037; and [f]Skaggs School of Pharmacy and Pharmaceutical Sciences, University of California, San Diego, La Jolla, CA 92093

Edited by Fred W. McLafferty, Cornell University, Ithaca, NY, and approved July 29, 2013 (received for review June 4, 2013)

There is immense cellular and molecular heterogeneity in biological systems. Here, we demonstrate the utility of integrating an inverted light microscope with an ambient ionization source, nanospray electrospray desorption ionization, attached to a high-resolution mass spectrometer to characterize the molecular composition of mouse spinal cords. We detected a broad range of molecules, including peptides and proteins, as well as metabolites such as lipids, sugars, and other small molecules, including *S*-adenosyl methionine and glutathione, through top-down MS. Top-down analysis revealed variation in the expression of Hb, including the transition from fetal to adult Hb and heterogeneity in Hb subunits consistent with the genetic diversity of the mouse models. Similarly, temporal changes to actin-sequestering proteins β-thymosins during development were observed. These results demonstrate that interfacing microscopy with ambient ionization provides the means to perform targeted in situ ambient top-down mass spectral analysis to study the pattern of proteins, lipids, and sugars in biologically heterogeneous samples.

ambient MS | top-down MS analysis | light microscopy | embryogenesis | central nervous system

Light microscopy has been instrumental to understanding biological processes, such as embryonic development, by providing insight into the temporal and spatial arrangements of cells within a tissue, but it provides limited molecular information. MS, in contrast, can provide detailed molecular information. However, if one aims to understand biology at multiple levels of organization, from molecules to organelles and, eventually, to entire organisms, methods that can bridge these levels and surpass the limitations of current techniques need to be developed. Most methods in biology examine a limited number of molecules at a time. As the need for system-wide analysis is emerging, so is the need for tools that can capture a wide range of chemistry. For example, immunohistochemistry yields excellent subcellular resolution of the distribution of the recognized antigen, but its applicability is limited mostly to certain peptides and proteins for which accurate and selective antibodies have been developed (1). By comparison, MS-based approaches, particularly MALDI-TOF imaging mass spectrometry (IMS), have demonstrated their capacity to explore the molecular nature of biology by integrating the chemistry of samples with their biology in a spatial manner (2–5). The quality of the spectra in MALDI-TOF imaging is dependent on very even and reproducible crystalline matrix deposition that limits transparency, and therefore the use of simultaneous microscopic analysis. A MALDI-TOF mass spectrometer has been built with a microscope, with which one can collect MALDI data and microscopy on the same sample (5). The design includes a stage where the topographic data are first collected by microscopy; the stage is then moved into position for MALDI-MS data collection, thereby disconnecting the microscopy step from mass spectrometric analysis even though both are present in the same instrument (5). In addition, the ease of obtaining and the quality of MALDI-TOF–based fragmentation, usually via postsource decay or a derivative thereof, have yet to be improved compared with collision-induced fragmentation. Information-rich fragmentation data, which provides insight into the biology under investigation, is critical for the identification of the molecules.

Although other ambient methods exist that can be interfaced with imaging modalities, such as laser ablation/dissection (6) and atomic force microscopy (7), electrospray ionization (ESI) MS has added an alternative powerful tool to the system-level exploration of biological questions, particularly in terms of proteomics and atmospheric analysis (8–12). Recently, several ESI-based ambient ionization MS techniques have been developed, including desorption electrospray ionization (DESI) and nanospray desorption electrospray ionization (nanoDESI), each of which has been adapted to perform IMS (13–16). Of these ambient ionization methods, nanoDESI has a spatial resolution down to 12 μm and superb MS spectral resolution with good mass accuracy when combined with high-resolution spectrometry (15, 16). High mass accuracy and spectral resolving power are essential for accurately identifying the signals of biomolecules, a particularly difficult task in the case of large biomolecules. NanoDESI operates at ambient pressure and temperature, does not require a sensitive tissue preparation protocol, and has an uncomplicated instrumental setup that works at multiple angles, all of which make it an appropriate technique to integrate with light microscopes commonly used in biological studies while maintaining high sensitivity. Here, we present our hybrid design that integrates the nanoDESI ion source with a hybrid linear trap quadrupole Fourier transform ion cyclotron resonance (LTQ-FT-ICR) mass spectrometer and an inverted light microscope into a single platform. The design is shown in Fig. 1, and its use is demonstrated in Movie S1. For ease of discussion, we will

Significance

To improve targeted molecular characterization of biological samples, we have interfaced a light microscope with ambient ionization MS to perform microscopy-guided targeted mass spectrometric analysis. This tool was used to characterize a diverse set of biomolecules ranging from lipids, sugars, peptides to proteins with molecular masses ranging from ∼300 Da to 16 kDa. Each of these entities could be characterized using top-down analysis directly on developing mouse spinal cords. This technology will be applicable in diverse fields ranging from chemical biology, pathology, and microbiology to neuroscience, medicine, and agriculture.

Author contributions: J.C., S.L.P., E.R.M., and P.C.D. designed research; C.-C.H., N.M.W., M.H., T.P., and I.B. performed research; E.C.L. and E.R.M. contributed new reagents/analytic tools; C.-C.H. analyzed data; and C.-C.H., N.M.W., E.R.M., and P.C.D. wrote the paper.

The authors declare no conflict of interest.

This article is a PNAS Direct Submission.

Freely available online through the PNAS open access option.

[1]To whom correspondence should be addressed. E-mail: pdorrestein@ucsd.edu.

This article contains supporting information online at www.pnas.org/lookup/suppl/doi:10.1073/pnas.1310618110/-/DCSupplemental.

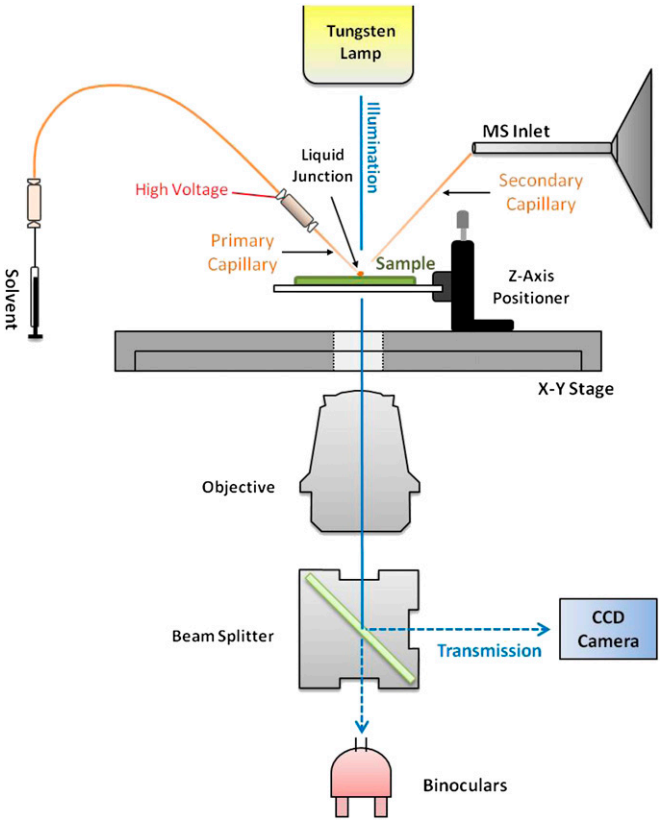

Fig. 1. Schematic overview of how targeted microscopy-based nanoDESI works. The light microscope is a modified Nikon DIAPHOT 300 inverted microscope. A home-built nanoDESI setup similar to that introduced by Watrous et al. (53) is integrated with the inverted microscope to perform in situ MS analysis. Thawed tissue sections on standard (1- × 3-inch) glass slides are positioned on a *z*-axis drive, which is fixed onto the *x*–*y* stage of the inverted microscope that is used to adjust the coordinate of the sample (relative to the nanoDESI liquid junction). The specimen is then moved under the liquid junction produced by the sampling capillaries so that the target sample region is directly underneath, as judged visually through the microscope, and desorbed molecules are aspirated into the secondary capillary. The ions in the electrospray process are generated at the terminal end of the secondary capillary, where the solvent is infused.

refer to the design described in this paper as ambient ionization interfaced with a microscope and mass spectometry (AMM).

The results that can be obtained with this hybrid instrument were first assayed using mouse frozen tissue sections. Previously, using MALDI-IMS and DESI, the molecular profiles during embryo development were performed on the tissue sections or preimplantation embryos (17–20). In an attempt to investigate the early development of the CNS, a mouse embryo was flash-frozen and sectioned at embryonic day (E) 15.5 after fertilization at the lumbar level of the developing spinal cord. Starting from a transmitted light image of the preparation positioned on the microscope, the spinal cord cross-section and adjacent structures were outlined, and mass spectra were obtained at locations of interest (Fig. 2). Spectra in the range of *m/z* 200–2,000 were obtained by FT-ICR-MS, with 50,000 resolving power. Three spectra, taken along the dorsoventral axis at locations 1, 2, and 3 noted on the histological image (Fig. 2*C*), are shown side by side in Fig. 2*A*. Within the selected range from ∼685–850 *m/z*, various classes of biomolecules were identified in each spectrum. Significantly different relative abundances were observed for several proteins at the selected locations (the process of identification of these proteins and molecules is described below and in *SI Appendix*). Indeed, high levels of the ions of two intact β-thymosins, thymosin β-10 (Tβ-10; 4,933.51 Da; 823.594 *m/z*, charge +6) and thymosin β-4 (Tβ-4; 4,960.48 Da; 828.098 *m/z*, charge +6) were observed in the spinal cord (Fig. 2*A*, spectrum 1) but were not detected in the body cavity (Fig. 2*A*, spectrum 3). A similar relative distribution was observed for ubiquitin (8,559.64 Da; 779.612 *m/z*, charge +11). A contrasting distribution pattern was observed for Hb, which was more abundant at location 3 in the body cavity than at location 1 in the spinal cord. Signals of monomeric Hb α-subunits (14,944.7–14,971.7 Da) and β-subunits (15,607.1 Da) predominated in the body cavity, which is rich in blood vessels in the E15.5 mouse embryo. The characterization of all proteins was determined by in situ top-down analysis using ProSight PTM (Kelleher lab, Northwestern University) as shown in Fig. 2*B* and *SI Appendix* (21–27). To support the annotation of Tβ-4 determined by top-down mass spectrometric analysis, we looked for Tβ-4 protein in a previously described global Tβ-4 KO mouse (28). The FT-MS spectra (Fig. 3) indicated Tβ-4 was not present in the Tβ-4 KO mouse, whereas Tβ-10 peaks were detected in both the WT and Tβ-4 KO samples. This was further supported by immunohistochemistry (*SI Appendix*, Fig. S17). This highlights the accuracy and sensitivity of this targeted microscopy MS interface. It also introduces the possibility that this technique could be used to identify a proteinaceous phenotype in genotypic mutants that display no obvious behavioral or cell biological phenotypes. In addition to proteins, metabolites were detected. Detected metabolites (Fig. 2*B*) were compared with metabolomic databases, such as METLIN (29) and MassBank (30). Phospholipids, the major component of cell membranes, such as phosphatidylcholine 34:1 (782.581 *m/z*, Na^+ adduct) and others with variable lipid chain lengths, were found throughout the sample, but the signal was significantly weaker in the cartilage primordium of the lumbar spine (we will refer to this as the cartilage primordium). In the lower *m/z* region, some of the critical small metabolites, such as glutathione (613.161 *m/z*), *S*-adenosyl methionine (399.146 *m/z*), and *L*-alpha-glycerylphosphorylcholine (Alpha-GPC, 296.068 *m/z*) were also observed in the spinal cord [*SI Appendix* (description of MS/MS spectra) and Fig. S1].

The transition of Hb from embryonic protein isoforms, known as fetal Hb, to adult isoforms is typically assayed by gel electrophoresis (31–33). Fetal Hb binds oxygen with greater affinity than does adult Hb, which allows the former to compete effectively for oxygen with adult Hb in the placental blood. High mRNA expression of mouse β-like fetal Hb, such as εy and βH1, has been reported at early embryonic stages (34). Given this known transition, we investigate the ontogeny of Hb isoforms during fetal and postnatal development [E12.5 to postnatal day (P) 10], as well as in the adult, using in situ top-down MS analysis to determine whether AMM is able to capture this by targeting the blood vessels adjacent to the spinal cord (*SI Appendix*, Movie S1). Using AMM, the monomeric Hb subunits, including the fetal β-like globins, were readily observed, as shown in Fig. 4. No intact tetrameric Hb ($\alpha_2\beta_2$) was observed, because the acid-induced ferrihemoglobin disassembly and heme (616.180 *m/z*; *SI Appendix*, Fig. S16) dissociation took place within subsecond intervals during real-time extraction from the tissue surface (35). As expected, the α-subunits were observed at all time points and the embryonic β-like Hb ε-Y2 subunit (16,004.4 Da) was found in all prenatal stages and disappeared at 2 d after birth (P2). In addition, the β-subunits were detected beginning at E13.5 (very low level compared with the other fetal Hb at E12.5) when they coexisted with ε-Y2. After gestation, the adult β-globin became the predominant form of β-like globin chains. Another fetal β-like globin, βH1 (16,352.6 Da), was also found on the E13.5 and E14.5 tissues, but it was not detected after E15.5. Our observation of high levels of ε-Y2 and βH1 β-like Hb in the prenatal stages is consistent with the transition from fetal Hb ($\alpha_2\varepsilon_2$ and $\alpha_2\beta h_2$) to adult Hb ($\alpha_2\beta_2$) reported (34).

In addition to capturing the developmental transition from fetal to adult Hb at the earlier time points, we observed heterogeneity of some documented adult α- and β-Hb proteoforms (e.g., α1: 14,944.7 Da, α2: 14,958.7 Da, α3: 14,971.7 Da, α4: 14,985.7 Da, α5: 15,000.7 Da; β1: 15,607.1 Da, β2: 15,699.1 Da) (36–38).

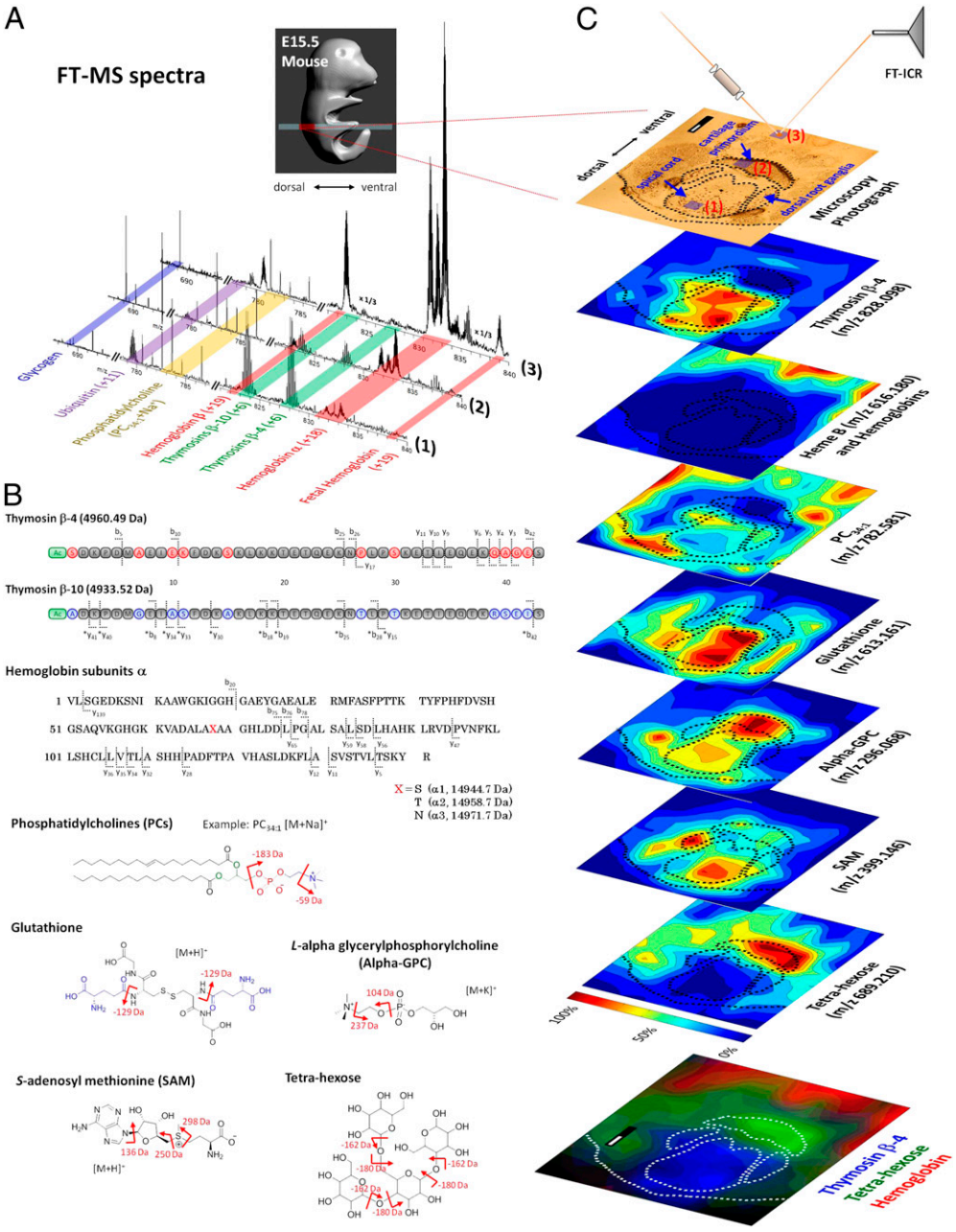

Fig. 2. AMM of an E15.5 mouse spinal cord section in the lumbar region. (*A*) High-resolution FT-MS spectra in the range of 685 to 850 *m/z* (*Lower*), taken at the locations specified by the blue squares depicted on the micrograph (*Upper*) along the dorsoventral axis: (*i*) the dorsal region of the spinal cord, (*ii*) the cartilage primordium, and (*iii*) the ventral body cavity. The regions of interest are outlined by the dotted lines. (*B*) Representative molecules, with molecular masses ranging from a few hundred Da to 15 kDa, are annotated via top-down tandem mass analysis (MS/MS spectra are described in *SI Appendix*). (*C*) Abundance contour maps reconstructed from a raster for several of the identified molecules. Heme, Hb. (Scale bar: 200 μm.)

This is a direct result of classical Mendelian genetics that affect hair color and the color of the eyes; in this case, the detected phenotype is the diversification of the observed molecular phenotype, the Hb proteoforms observed in the offspring when two parents mate. The annotations of the Hb ions were verified by matching *y* and *b* ions using the top-down approach with ProSight PTM (*SI Appendix*, Figs. S2–S7). Some other low-intensity ions that represent masses of ∼16 kDa were observed during the fetal period. These may yet represent other globins important during development, but they were not of sufficient abundance to get fragmentation information. These results highlight how top-down ambient mass spectrometric analysis can identify protein isoforms with sufficient specificity to provide valuable insight into the role distinct isoforms play in localized and temporally specific biological processes.

Having demonstrated that the interface of nanoDESI with light microscopy can capture molecular changes during embryonic development with top-down MS, we proceeded to use this approach to measure the spatial distribution of specific molecules in the spinal cord. Using the microscope to position the nanoDESI probe for data collection, FT-MS spectra were collected from the E15.5 tissue in a raster at locations spaced ∼160 μm apart from each other. Representative molecular contour maps of individual ions were plotted in a color scale representing the relative intensity of the specific *m/z* (Fig. 2*C*). It is notable that no significant protein signals above the detection limit were found on the cartilage primordium; however, a great amount of tetra-hexose (689.210 *m/z*), based on our interpretation of the MS^2 and MS^3 spectra (*SI Appendix*, Fig. S12), was detected near the cartilage primordium. As expected, Hb ions were absent from this area, given that cartilage is devoid of blood vessels. The two β-thymosins, as well as small metabolites, such as glutathione and Alpha-GPC, all showed slight but consistent dorsoventral asymmetrical distributions in the spinal cord. One of the molecules that displayed this asymmetry was S-adenosyl methionine (SAM), a metabolite known to affect transcriptional regulation through histone methylation (39, 40). The limit of detection of β-thymosins is at subfemtomole

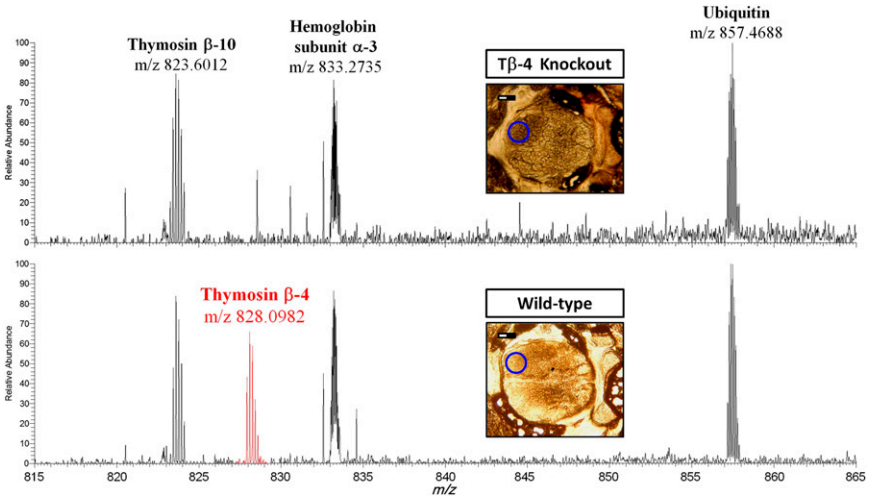

Fig. 3. Targeted AMM analysis of Tβ-4 KO mouse tissue sections. The FT-MS spectrum and microscope photographs of in situ Tβ-4 KO (*Upper*) and WT (*Lower*) P2 mice, using AMM, are shown. Spectra were collected on the spinal cords near the dorsal end, as indicated by the blue circles. (Scale bar: 200 μm.) The absence of the *m/z* 828.0982 ion clusters in the KO mouse verifies its annotation of Tβ-4 via the top-down approach.

levels (*SI Appendix*, Fig. S19). Although only abundant proteins were observed at this point, our result demonstrates that endogenous proteins can be resolved and characterized via top-down analysis directly from a tissue surface using ambient MS.

The β-thymosin isoforms Tβ-4 and Tβ-10 are both abundant in the developing CNS, as well as in proliferating tumor cells, and can be regulated by cell fate regulators, such as retinoic acid (41–44). β-thymosins are highly conserved polypeptides that act as actin-sequestering molecules and regulate the polymerization of G (globular) actin to form F (filamentous) actin (45–47). Altered expression of β-thymosins is strongly associated with various important biological activities, especially tissue repair and regeneration (42, 43). Given the significant developmental transitions in Hb isoforms, we sought to explore whether such changes were also associated with key β-thymosins. Our spatiotemporal results indicate that from early embryonic stages to P10, both Tβ-4 and Tβ-10 are detected in and near the spinal cord (Fig. 5). At the earliest embryonic stage studied (E12.5), the distributions of Tβ-4 and Tβ-10 both display dorsally low-to-ventrally high concentration gradients, with increased levels around the notochord. Similar concentration gradients were also found at E13.5 for both Tβ-4 and Tβ-10; however, at and after E15.5, the signals for both thymosins on the cartilage primordium diminish. At stages later than E12.5, the ions for β-thymosins become more intense within the spinal cord.

The data suggest that Tβ-10 is depleted more rapidly than Tβ-4 during embryogenesis. To ensure this is not an artifact of ionization, an instrumental response plot using synthetic β-thymosin standards was obtained (*SI Appendix*, Fig. S19). The ion intensity ratio of Tβ10 to Tβ4 (γ) had a linear relationship to the relative amount of the two β-thymosins using the AMM and indicated there was no ionization bias when the two thymosins were compared. Based on this result, we proceeded to investigate the relative spatiotemporal features of the two β-thymosins. A linear trend of γ at E12.5 (Fig. 5) revealed a gradient along the dorsoventral axis, high near the notochord (γ ∼1.6) and low near the roof plate (γ = 0.4). At 6 d before birth (E13.5), a similar dorsoventral gradient of γ-values persisted in the spinal cord, but the gradients became less significant starting from E14.5. Then, at E15.5 and P2, the γ-values of all sampling points throughout the spinal cord approached ∼1.0. After birth, the relative amount of Tβ-10 decreased and became completely undetectable with AMM in the adult spinal cord. Compared with Tβ-4, Tβ-10 levels dropped significantly within 10 d after birth, as shown by the low

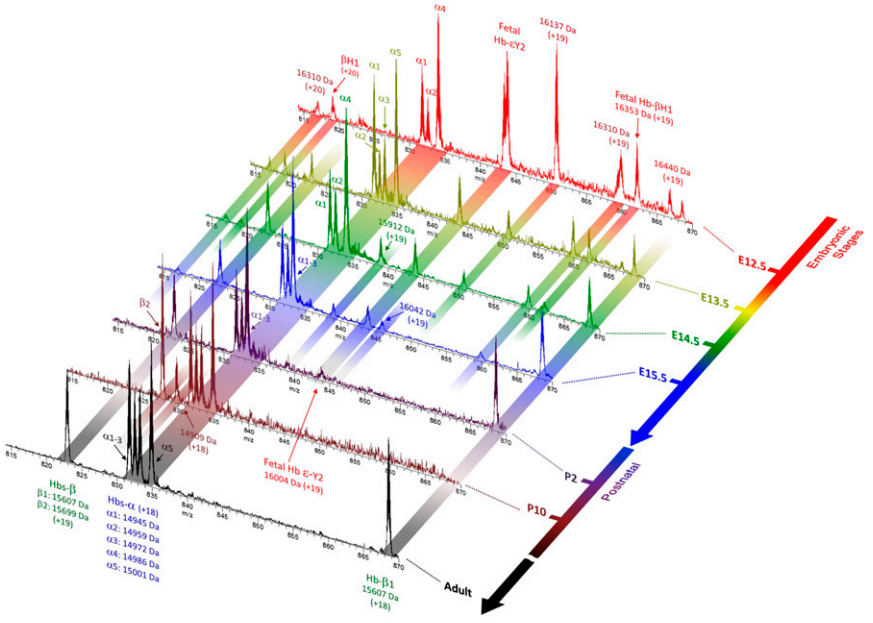

Fig. 4. Mouse Hb expression during development characterized by AMM. All the FT-MS spectra were taken by targeted analysis of the blood vessel-rich regions of the tissue sections near the spinal cord. The data show that the variety of Hb subtypes and isoforms over time can be captured using this approach. Proteins that were not identified by top-down analysis are labeled by the corresponding monoisotopic masses and charge states (in parentheses). Heterogeneity of adult α-Hb and β-Hb isoforms (e.g., absence of α4 in E13.5 and α5 in E12.5, β2 instead of β1 in P10) results from the genetic diversity inherent in the parental background strains, which is then passed to their offspring. Replicates of E12.5–P2 using different mice are displayed in *SI Appendix*, Fig. S21.

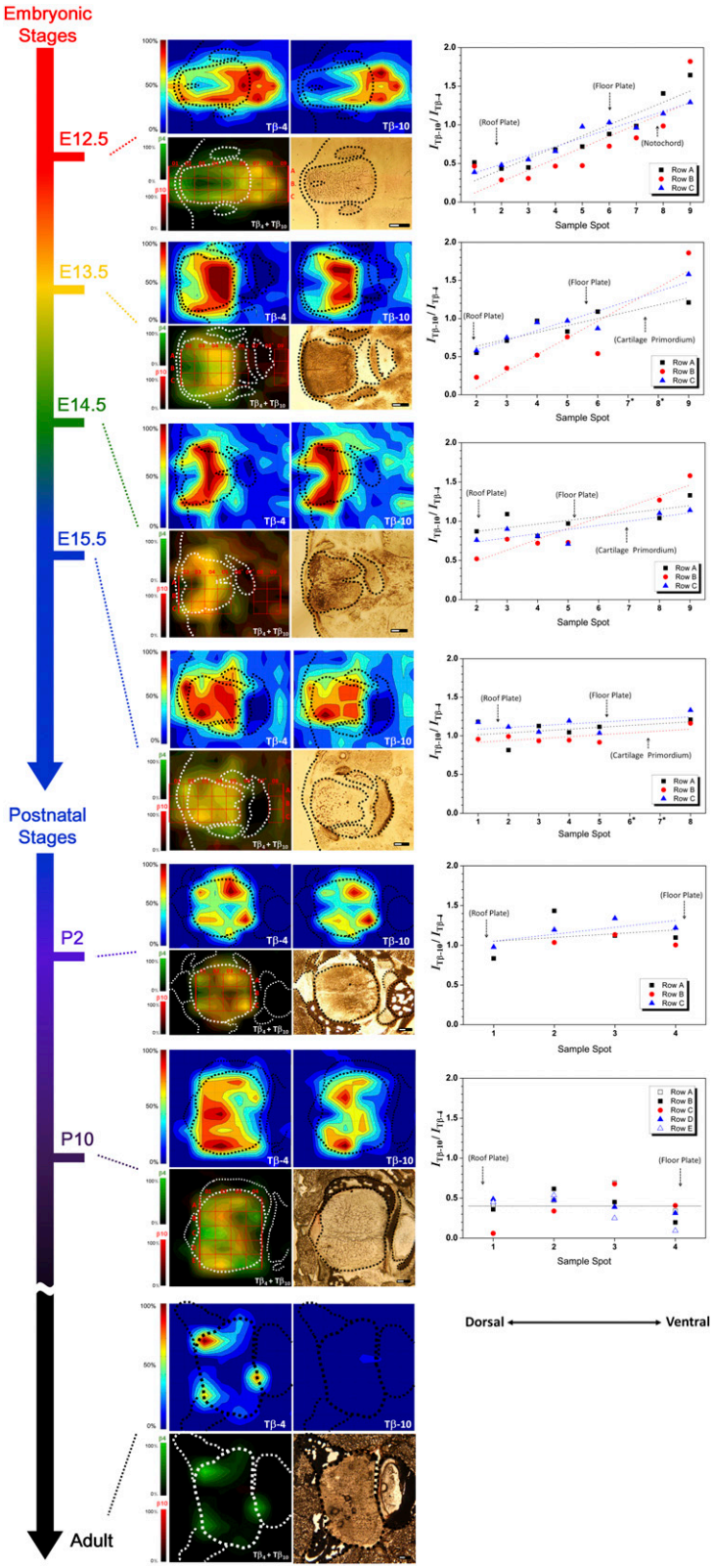

Fig. 5. Contour maps of Tβ-4 and Tβ-10 in spinal cord sections during embryonic development and the transition from prenatal to adult mice. Molecular contour maps of Tβ-4 (*Upper Left*, rainbow scale), Tβ-10 (*Upper Right*, rainbow scale), overlays of both [*Lower Right*, Tβ-4 (green) and Tβ-10 (red)], and transparent photographs at the indicated embryonic stages taken with the microscope (*Lower Left*) are shown. The dashed lines represent histological outlines. The red grids (*Left*) indicate the sample spots at which the ion intensity ratios of Tβ-10/Tβ-4 were plotted along the dorsoventral axes that are shown (*Right*). Because very low β-thymosin signals were detected on the cartilage primordium (prenatal) and vertebrae (postnatal) starting at E13.5, ratios of those sampling spots were not presented. The lines indicate the general ratio trend observed in the data. (Scale bar: 200 μm.) Replicates of E12.5–P2 are displayed in *SI Appendix*, Fig. S20.

γ-plot at P10. This rapid decrease relative to Tβ-4 is consistent with the drop observed in the developing brain at postnatal stages (41). Thus, AMM reveals gradients of molecules in the spinal cord during embryonic development. Such gradients have not been reported for β-thymosins or any of the other molecules that were detected, such as SAM or glutathione. Many morphogens, such as sonic hedgehog, display concentration gradients during embryonic development and are thought to determine cell fate via transcriptional regulation (48–52). Based on the initial data obtained with AMM, we hypothesize that the regulation of β-thymosins plays a role in embryonic spinal cord development, perhaps through binding of G-actin (41, 45).

In conclusion, we propose that the nanoDESI/microscope MS interface, a unique approach that provides targeted molecular information, can be used to reveal molecular changes over time and space, genotypic information, and subtle molecular phenotypes in real time. Although AMM is applied to study tissues in this work, other types of samples that are amenable to microscopy could also be analyzed using this technique. We foresee novel applications of this methodology in areas ranging from chemical biology, pathology, and microbiology to neuroscience, medicine, and agriculture.

Methods

The details of the operation and design of AMM, the methods for top-down mass spectrometry, and the databases consulted can be found in *SI Methods*.

ACKNOWLEDGMENTS. We thank Karen Lettieri, Laura Franco, Onanong Chivatakarn, and other members of the laboratory of S.L.P. for technical assistance. We also thank Dr. Michael Baker in the laboratory of E.R.M. for additional assistance with instrument development. Input from all members of the laboratory of P.C.D. is greatly appreciated. Research in the laboratory of P.C.D. for the development of real-time MS was supported by National Institutes of Health Grant GM094802. The work in the laboratory of E.R.M. was supported by National Science Foundation Grant DBI-0852081. The work in the laboratory of S.L.P. studying the spinal cord was supported by National Institute of Neurological Disorders and Stroke Grant R37NS037116, the Marshall Heritage Foundation, and the Howard Hughes Medical Institute (HHMI). M.H. is supported by the Timken–Sturgis Foundation and the Japanese Ministry of Education, Culture, Sports, Science, and Technology Long-Term Student Support Program. S.L.P. is an HHMI investigator.

1. Ramos-Vara JA (2005) Technical aspects of immunohistochemistry. *Vet Pathol* 42(4): 405–426.
2. Caprioli RM, Farmer TB, Gile J (1997) Molecular imaging of biological samples: Localization of peptides and proteins using MALDI-TOF MS. *Anal Chem* 69(23):4751–4760.
3. Cornett DS, Reyzer ML, Chaurand P, Caprioli RM (2007) MALDI imaging mass spectrometry: Molecular snapshots of biochemical systems. *Nat Methods* 4(10):828–833.
4. Seeley EH, Caprioli RM (2008) Molecular imaging of proteins in tissues by mass spectrometry. *Proc Natl Acad Sci USA* 105(47):18126–18131.
5. Harada T, et al. (2009) Visualization of volatile substances in different organelles with an atmospheric-pressure mass microscope. *Anal Chem* 81(21):9153–9157.
6. Lorenz M, Ovchinnikova OS, Kertesz V, Van Berkel GJ (2013) Laser microdissection and atmospheric pressure chemical ionization mass spectrometry coupled for multimodal imaging. *Rapid Commun Mass Spectrom* 27(13):1429–1436.
7. Ovchinnikova OS, Nikiforov MP, Bradshaw JA, Jesse S, Van Berkel GJ (2011) Combined atomic force microscope-based topographical imaging and nanometer-scale resolved proximal probe thermal desorption/electrospray ionization-mass spectrometry. *ACS Nano* 5(7):5526–5531.
8. Aebersold R, Mann M (2003) Mass spectrometry-based proteomics. *Nature* 422(6928): 198–207.
9. Olsen JV, et al. (2006) Global, in vivo, and site-specific phosphorylation dynamics in signaling networks. *Cell* 127(3):635–648.
10. Zanivan S, et al. (2008) Solid tumor proteome and phosphoproteome analysis by high resolution mass spectrometry. *J Proteome Res* 7(12):5314–5326.
11. Domon B, Aebersold R (2006) Mass spectrometry and protein analysis. *Science* 312(5771):212–217.
12. Grassmann J, Scheerle RK, Letzel T (2012) Functional proteomics: Application of mass spectrometry to the study of enzymology in complex mixtures. *Anal Bioanal Chem* 402(2):625–645.
13. Takáts Z, Wiseman JM, Gologan B, Cooks RG (2004) Mass spectrometry sampling under ambient conditions with desorption electrospray ionization. *Science* 306(5695):471–473.
14. Badu-Tawiah AK, Eberlin LS, Ouyang Z, Cooks RG (2013) Chemical aspects of the extractive methods of ambient ionization mass spectrometry. *Annu Rev Phys Chem* 64:481–505.
15. Laskin J, Heath BS, Roach PJ, Cazares L, Semmes OJ (2012) Tissue imaging using nanospray desorption electrospray ionization mass spectrometry. *Anal Chem* 84(1): 141–148.
16. Eckert PA, Roach PJ, Laskin A, Laskin J (2012) Chemical characterization of crude petroleum using nanospray desorption electrospray ionization coupled with high-resolution mass spectrometry. *Anal Chem* 84(3):1517–1525.
17. Burnum KE, et al. (2008) Imaging mass spectrometry reveals unique protein profiles during embryo implantation. *Endocrinology* 149(7):3274–3278.
18. Burnum KE, et al. (2009) Spatial and temporal alterations of phospholipids determined by mass spectrometry during mouse embryo implantation. *J Lipid Res* 50(11):2290–2298.
19. Ferreira CR, Pirro V, Eberlin LS, Hallett JE, Cooks RG (2012) Developmental phases of individual mouse preimplantation embryos characterized by lipid signatures using desorption electrospray ionization mass spectrometry. *Anal Bioanal Chem* 404(10): 2915–2926.
20. Ferreira CR, Eberlin LS, Hallett JE, Cooks RG (2012) Single oocyte and single embryo lipid analysis by desorption electrospray ionization mass spectrometry. *J Mass Spectrom* 47(1):29–33.
21. Loo JA, et al. (1992) High-resolution tandem mass spectrometry of large biomolecules. *Proc Natl Acad Sci USA* 89(1):286–289.
22. Senko MW, Speir JP, McLafferty FW (1994) Collisional activation of large multiply charged ions using Fourier transform mass spectrometry. *Anal Chem* 66(18):2801–2808.
23. Kelleher NL, et al. (1999) Top down versus bottom up protein characterization by tandem high-resolution mass spectrometry. *J Am Chem Soc* 121(4):806–812.
24. Ge Y, et al. (2002) Top down characterization of larger proteins (45 kDa) by electron capture dissociation mass spectrometry. *J Am Chem Soc* 124(4):672–678.
25. Kelleher NL (2004) Top-down proteomics. *Anal Chem* 76(11):197A–203A.
26. Chait BT (2006) Chemistry. Mass spectrometry: Bottom-up or top-down? *Science* 314(5796):65–66.
27. LeDuc RD, et al. (2004) ProSight PTM: An integrated environment for protein identification and characterization by top-down mass spectrometry. *Nucleic Acids Res* 32(Web Server issue):W340–W345.
28. Banerjee I, et al. (2012) Thymosin beta 4 is dispensable for murine cardiac development and function. *Circ Res* 110(3):456–464.
29. Smith CA, et al. (2005) METLIN: A metabolite mass spectral database. *Ther Drug Monit* 27(6):747–751.
30. Horai H, et al. (2010) MassBank: A public repository for sharing mass spectral data for life sciences. *J Mass Spectrom* 45(7):703–714.
31. Barrowman J, Craig M (1961) Haemoglobins of foetal C57BL/6 mice. *Nature* 190(4778): 818–819.
32. Stamatoyannopoulos G (2001) *The Molecular Basis of Blood Diseases*, eds Stamatoyannopoulos G, Majerus PW, Perlmutter RM, Varmus H (Saunders, Philadelphia), pp 135–182.
33. Manning JM, Popowicz AM, Padovan JC, Chait BT, Manning LR (2012) Intrinsic regulation of hemoglobin expression by variable subunit interface strengths. *FEBS J* 279(3):361–369.
34. Trimborn T, Gribnau J, Grosveld F, Fraser P (1999) Mechanisms of developmental control of transcription in the murine α- and β-globin loci. *Genes Dev* 13(1):112–124.
35. Simmons DA, Wilson DJ, Lajoie GA, Doherty-Kirby A, Konermann L (2004) Subunit disassembly and unfolding kinetics of hemoglobin studied by time-resolved electrospray mass spectrometry. *Biochemistry* 43(46):14792–14801.
36. Popp RA (1967) Hemoglobins of mice: Sequence and possible ambiguity at one position of the alpha chain. *J Mol Biol* 27(1):9–16.
37. Popp RA, Bailiff EG, Skow LC, Whitney JB, 3rd (1982) The primary structure of genetic variants of mouse hemoglobin. *Biochem Genet* 20(1-2):199–208.
38. Popp RA (1973) Sequence of amino acids in the chain of single hemoglobins from C57BL, SWR, and NB mice. *Biochim Biophys Acta* 303(1):52–60.
39. Shyh-Chang N, et al. (2013) Influence of threonine metabolism on S-adenosylmethionine and histone methylation. *Science* 339(6116):222–226.
40. Lilja T, Heldring N, Hermanson O (2013) Like a rolling histone: Epigenetic regulation of neural stem cells and brain development by factors controlling histone acetylation and methylation. *Biochim Biophys Acta* 1830(2):2354–2360.
41. Lugo DI, et al. (1991) Developmental regulation of beta-thymosins in the rat central nervous system. *J Neurochem* 56(2):457–461.
42. Sribenja S, et al. (2009) Advances in thymosin beta10 research: Differential expression, molecular mechanisms, and clinical implications in cancer and other conditions. *Cancer Invest* 27(10):1016–1022.
43. Goldstein AL, Hannappel E, Sosne G, Kleinman HK (2012) Thymosin β4: A multifunctional regenerative peptide. Basic properties and clinical applications. *Expert Opin Biol Ther* 12(1):37–51.
44. Hall AK, Hempstead J, Morgan JI (1990) Thymosin beta 10 levels in developing human brain and its regulation by retinoic acid in the HTB-10 neuroblastoma. *Brain Res Mol Brain Res* 8(2):129–135.
45. Yu FX, Lin SC, Morrison-Bogorad M, Atkinson MAL, Yin HL (1993) Thymosin beta 10 and thymosin beta 4 are both actin monomer sequestering proteins. *J Biol Chem* 268(1):502–509.
46. Huff T, Müller CSG, Otto AM, Netzker R, Hannappel E (2001) beta-Thymosins, small acidic peptides with multiple functions. *Int J Biochem Cell Biol* 33(3):205–220.
47. Mannherz HG, Hannappel E (2009) The beta-thymosins: intracellular and extracellular activities of a versatile actin binding protein family. *Cell Motil Cytoskeleton* 66(10): 839–851.
48. Balaskas N, et al. (2012) Gene regulatory logic for reading the Sonic Hedgehog signaling gradient in the vertebrate neural tube. *Cell* 148(1-2):273–284.
49. Jessell TM (2000) Neuronal specification in the spinal cord: Inductive signals and transcriptional codes. *Nat Rev Genet* 1(1):20–29.
50. Briscoe J, et al. (1999) Homeobox gene Nkx2.2 and specification of neuronal identity by graded Sonic hedgehog signalling. *Nature* 398(6728):622–627.
51. Chamberlain CE, Jeong J, Guo C, Allen BL, McMahon AP (2008) Notochord-derived Shh concentrates in close association with the apically positioned basal body in neural target cells and forms a dynamic gradient during neural patterning. *Development* 135(6):1097–1106.
52. Sasaki N, Kurisu J, Kengaku M (2010) Sonic hedgehog signaling regulates actin cytoskeleton via Tiam1-Rac1 cascade during spine formation. *Mol Cell Neurosci* 45(4): 335–344.
53. Watrous J, et al. (2012) Mass spectral molecular networking of living microbial colonies. *Proc Natl Acad Sci USA* 109(26):E1743–E1752.